Modeling Alternation to Synchrony with Inhibitory Coupling: A Neuromorphic VLSI Approach

Gennady S. Cymbalyuk
Institute of Mathematical Problems in Biology, Russian Academy of Sciences, Push-chino, Moscow region, Russia 142292, and Department of Biology, Emory University, Atlanta, Georgia 30322, U.S.A

Girish N. Patel
School of Electrical and Computer Engineering, Georgia Institute of Technology, Atlanta, Georgia 30332-0250, U.S.A.

Ronald L. Calabrese
Department of Biology, Emory University, Atlanta, Georgia 30322, U.S.A.

Stephen P. DeWeerth
School of Electrical and Computer Engineering, Georgia Institute of Technology, Atlanta, Georgia 30332-0250, U.S.A.

Avis H. Cohen
Department of Biology, University of Maryland, College Park, Maryland 20742, U.S.A.

We developed an analog very large-scale integrated system of two mutually inhibitory silicon neurons that display several different stable oscillations. For example, oscillations can be synchronous with weak inhibitory coupling and alternating with relatively strong inhibitory coupling. All oscillations observed experimentally were predicted by bifurcation analysis of a corresponding mathematical model. The synchronous oscillations do not require special synaptic properties and are apparently robust enough to survive the variability and constraints inherent in this physical system.

In biological experiments with oscillatory neuronal networks, blockade of inhibitory synaptic coupling can sometimes lead to synchronous oscillations. An example of this phenomenon is the transition from alternating to synchronous bursting in the swimming central pattern generator of lamprey when synaptic inhibition is blocked by strychnine. Our results suggest a simple explanation for the observed oscillatory transitions in the lamprey central pattern generator network: that inhibitory connectivity alone is sufficient to produce the observed transition.

1 Introduction

Experimental studies, especially in the realm of central pattern generators (CPGs), have emphasized the importance of reciprocal inhibitory connections in producing alternating oscillations, whereas excitatory connections or electrical connections are thought to mediate synchronous oscillations. The potential synchronizing role of weak inhibitory connections is often disregarded. However, when the strength of inhibitory connections is reduced by experimental treatments in some preparations, a transition from alternation to synchronization has been observed. A particularly relevant example of this type of transition is provided by experiments with the lamprey spinal cord (Cohen & Harris-Warrick, 1984; Alford, Sigvardt, & Williams, 1990). The segmental CPGs of the lamprey swim system are composed of two reciprocally inhibitory units that represent oscillatory neural networks located on contralateral sides of the spinal cord. The oscillations in the units are based on intrinsic membrane and circuit properties. Under normal conditions, the two units oscillate in antiphase. However, in the presence of strychnine, which blocks glycinergic inhibitory coupling, they oscillate synchronously (Cohen & Harris-Warrick, 1984; Alford et al., 1990).

Theoretical studies of oscillatory neural networks have shown that inhibitory connections can lead to synchronization (Lytton & Sejnowski, 1991; Wang & Rinzel, 1993; Destexhe, Contreras, Sejnowski, & Stereade, 1994; Golomb, Wang, & Rinzel, 1994; Borisyuk, Borisyuk, Khibnik, & Roose, 1995; Bush & Sejnowski, 1996; White, Chow, Ritt, Soto-Treviño, & Kopell, 1998; Chow, White, Ritt, & Kopell, 1998; Rubin & Terman, 2000). In particular, mutually inhibitory connections in a two-cell system can produce stable synchronous oscillations in some regimes of parameter space. In the limit of weak coupling, asymptotic methods are useful in finding phase-locked periodic solutions and determining their stability (Malkin, 1956; Blechman, 1981; Kuramoto, 1984; Ermentrout & Kopell, 1991; Cymbalyuk, Nikolaev, & Borisyuk, 1994; Hoppensteadt & Izhikevich, 1997). It has been emphasized that in order to synchronize oscillations, some parameters such as rate of rise or decay of synaptic coupling should be sufficiently slow with respect to the spike waveform (Wang & Rinzel, 1992; Van Vreeswijk, Abbot, & Ermentrout, 1994; Gerstner, van Hemmen, & Cowan, 1996; Terman, Kopell, & Bose, 1998). Also, insight about the synchronization properties of a system of oscillatory neurons can be gained by characterizing the intrinsic membrane properties of the component neurons by establishing their phase-response curve type (Hansel, Mato, & Meunier, 1995; Ermentrout, 1996; Hoppensteadt & Izhikevich, 1997; Rinzel & Ermentrout, 1998; Izhikevich, 1999).

However, some behaviors observed in mathematical models may not be observed in real systems due to constraints imposed by the physical world. For example, a parameter regime corresponding to synchronous oscillations in a given model may be so narrow that noise in the system

or mismatch among the oscillators prevents a reliable observation of this particular behavior.

For this article, we conducted experiments with silicon neurons to test the robustness of different oscillatory regimes observed in a corresponding mathematical model. We have implemented neural oscillators using neuromorphic very large-scale integrated (VLSI) circuits that are fabricated in standard silicon microelectronic processes (Mead, 1989; Patel, Cymbalyuk, Calabrese, & DeWeerth, 1999). In addition, we have derived a mathematical model describing the silicon neuron's dynamic properties (Patel et al., 1999). Using a system of two mutually inhibitory connected silicon neurons, we demonstrate stable synchronous oscillations as well as other behaviors predicted by the mathematical model. Thus, the dynamic behaviors revealed in the experiments are sufficiently robust to persist under the physical constraints inherent in silicon neuron technology. These experimental observations help to build intuitions as to how such behaviors may be observed in experiments with real neurons.

We show that a physical system of two silicon neurons can display stable synchronous oscillations with weak inhibitory coupling, thus realizing the predictions developed by exploring a corresponding mathematical model. These synchronous oscillations do not require synaptic connections possessing significant delay, or slow rise and decay properties, and are sufficiently robust to survive the physical constraints. We suggest a simple explanation for the observed oscillatory transitions in the lamprey CPG network: that inhibitory connectivity alone is sufficient to produce the observed transition.

2 Silicon Neuron

We have implemented a silicon neuron (Patel & DeWeerth, 1997; Patel et al., 1999) inspired by a mathematical model of an excitable cell (Morris & Lecar, 1981). The mathematical model describes the dynamics of a neuron possessing an inward Ca^{2+} current with instantaneous activation dynamics, an outward K^+ current with slow activation dynamics, and a leak current. This model appears to be at a reasonable level of reduction of the neuronal dynamics reconciling relative simplicity of analysis with biophysical plausibility (Rinzel & Ermentrout, 1998; Skinner, Turrigiano, & Marder, 1993).

The design of our silicon neuron is based on subthreshold operation of MOS (metal-oxide-semiconductor) transistors and the current-mode techniques described by Mahowald and Douglas (1991). The basic building block is a voltage-controlled conductor implemented with a single MOS transistor. A pair of complementary MOS transistors is shown in Figures 1A and 1B. The I-V characteristics of the voltage-controlled conductor, implemented with an n-type MOS transistor (see Figure 1A), is described by

$$I_D = I_0 e^{(\kappa V_G - V_S)/U_T}(1 - e^{-V_{DS}/U_T}), \tag{2.1}$$

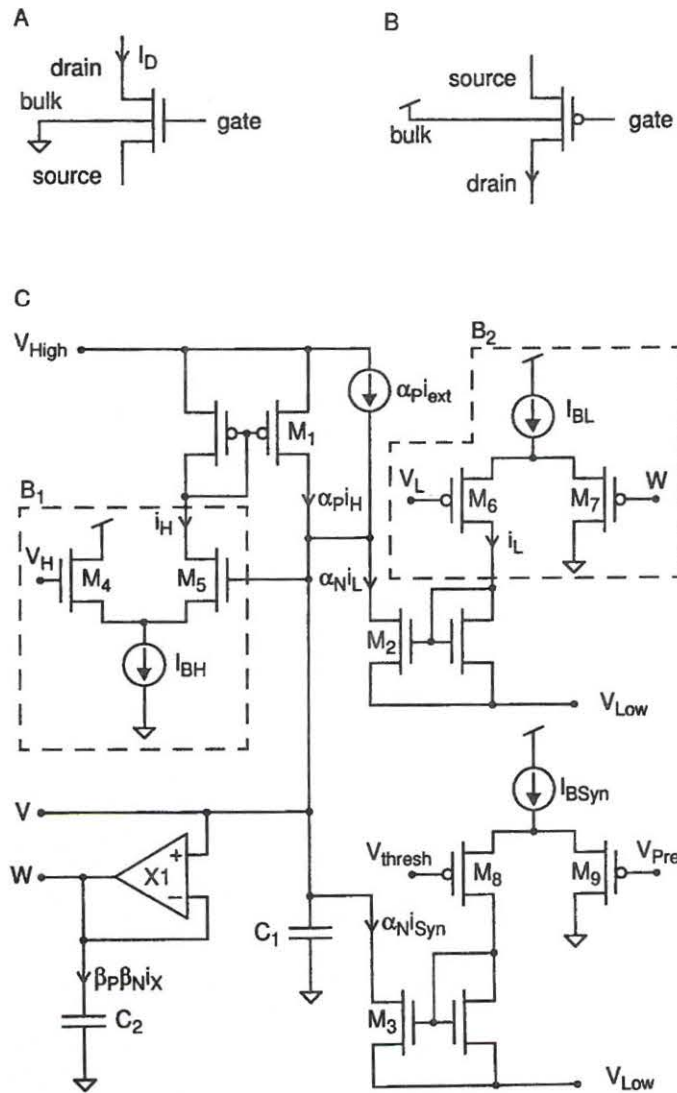Cymbalyuk, Patel, Calabrese, DeWeerth, & Cohen

Figure 1: Building blocks and circuit schematic of the silicon neuron. (A) n-type and (B) p-type MOS transistors are used as conductors. The bulk node of a transistor, which is usually not displayed, is the fourth terminal of MOS transistors. The bulk nodes of n-MOS transistors are typically connected to the lowest potential in the circuit (Gnd), and the bulk nodes of p-MOS are connected to highest potential in the circuit (V_{dd}). (C) Circuit schematic of the silicon neuron. Transistors M_1, M_2 and M_3 emulate voltage-gated calcium, potassium, and synaptic currents, respectively.

where I_D is the drain-to-source current, I_0 and κ are physical constants that depend on the fabrication process, U_T is the thermal voltage (kT/q), V_G and V_S are the gate and source voltages with respect to the bulk node, and V_{DS} is the drain-to-source voltage (Mead, 1989). The drain-to-source current of the complementary pMOS transistor (see Figure 1B) is also described by equation 2.1; however, the signs of all voltages are reversed. For both nMOS and pMOS transistors, the gate current is zero. For $V_{DS} \gg U_T$, the transistor operates in its saturation region where the drain-to-source current is given by

$$I_{SAT} \approx I_0 e^{(\kappa V_G - V_S)/U_T}. \tag{2.2}$$

For $V_{DS} \ll U_T$ and a fixed value of V_{GS} (gate-to-source voltage), the transistor operates in its ohmic region where the I-V characteristic is approximately linear:

$$I_{ohmic} \approx I_{SAT} \frac{V_{DS}}{U_T}. \tag{2.3}$$

The schematic diagram of the silicon neuron is shown in Figure 1C. The voltage across the capacitors C_1 is the state variable representing the membrane potential, V, and the voltage across the capacitors C_2 is the slow-state variable corresponding to activation of K^+ current, W.

Current conservation at node V yields

$$C_1 \dot{V} = \alpha_P i_H - \alpha_N i_L + \alpha_P I_{ext}, \tag{2.4}$$

where $\alpha_P i_H$, $\alpha_N i_L$ correspond to the Ca^{2+} and K^+ currents, respectively, and I_{ext} is an externally applied current. Currents i_H and i_L are the output currents of the differential pair circuits enclosed in the dashed boxes B_1 and B_2, respectively. α_P and α_N describe the ohmic effects of transistors M_1 and M_2, respectively. In our implementation, there is no membrane leak current. Current conservation at node W yields

$$C_2 \dot{W} = \beta_P \beta_N i_x, \tag{2.5}$$

where i_x is the output current of the operational transconductance amplifier (OTA) and β_P and β_N represent the ohmic effects of pull-up and pull-down transistors inside the OTA. The output currents of a differential pair circuit and an OTA circuit, derived by using equation 2.2, are described by a Fermi function and a hyperbolic tangent function, respectively (Mead, 1989). Substituting these functions into equations 2.4 and 2.5 yields

$$C_1 \dot{V} = f(V, W) = I_{ext} \alpha_P + I_{BH} \frac{e^{\kappa(V - V_H)/U_T}}{1 + e^{\kappa(V - V_H)/U_T}} \alpha_P$$

$$-I_{BL}\frac{e^{\kappa(W-V_L)/U_T}}{1+e^{\kappa(W-V_L)/U_T}}\alpha_N, \tag{2.6}$$

$$C_2\dot{W} = I_\tau \tanh\left(\kappa\frac{V-W}{2U_T}\right)\beta_P\beta_N, \tag{2.7}$$

where

$$\alpha_P = 1 - e^{((V-V_{High})/U_T)}, \tag{2.8}$$

$$\alpha_N = 1 - e^{((V_{Low}-V)/U_T)}, \tag{2.9}$$

$$\beta_P = 1 - e^{((W-V_{dd})/U_T)}, \tag{2.10}$$

$$\beta_N = 1 - e^{(-W/U_T)}. \tag{2.11}$$

In the above formulation, the bulk nodes of nMOS and pMOS transistors are connected to V_{Low} and V_{High}, respectively.

As shown in Figure 1C, an inhibitory synapse is implemented with a single nMOS transistor, M_3, whose gate voltage is determined by the drain-to-source current of M_8. The synaptic current i_{Syn} responds to changes in the presynaptic potential instantaneously. For a neuron with a single inhibitory synapse, equation 2.6 is modified as follows:

$$C_1\dot{V} = f(V, W) - i_{Syn}, \tag{2.12}$$

where $f(V, W)$ is given in equation 2.6 and

$$i_{Syn} = \alpha_N I_{BSyn}\left(\frac{e^{\kappa(V_{pre}-V_{thresh})/U_T}}{1+e^{\kappa(V_{pre}-V_{thresh})/U_T}}\right). \tag{2.13}$$

In equation 2.13, V_{pre} corresponds to the membrane potential of the presynaptic neuron, α_N is given in equation 2.9, and I_{BSyn} represents the maximal synaptic conductance.

3 Experimental Characterization of the Model

We focused our experiments on the quantification of observed behaviors in a two-cell silicon neuron network connected by mutually inhibitory synapses along with the characterization of the corresponding mathematical model. The observed behaviors were quantified by sampling the voltage waveforms (approximately 20 periods' worth) and postprocessing the data. The oscillatory behaviors were studied while I_{BSyn} was varied from approximately 5 pA to 1 μA. The parameters of the silicon neuron were set so that each neuron, in the absence of synaptic coupling, behaved as an oscillator.

Most of the parameters in the mathematical model of the silicon neuron were measured experimentally. Three others were inaccessible for measurements. These were estimated based on the circuit design and adjusted to fit

the experimental data. Directly measured parameters were V_{High}, V_{Low}, V_H, and V_{dd}. Current sources I_{BH} and I_{BL} were measured in voltage-clamp experiments via the membrane potential node. The value of $\kappa = 0.65$ was determined by measuring the slope of the steady-state activation curve of the inward current. At room temperature, U_T is approximately 0.025 volts. The values of C_1 and C_2 were determined by matching the period of oscillations observed in the silicon model with that observed in the mathematical model. Because W is an inaccessible node, we estimate the value of I_τ by assuming current sources I_{BH} and I_τ match to within an order of magnitude. The exact value of I_τ was chosen to match the bifurcation diagram resulting from experimental data to that computed from the mathematical model.[1]

Through a series of voltage-clamp experiments, we characterized the synaptic coupling in our model neuron. By turning off all current sources except I_{BSyn} and clamping V to a constant voltage, the current at the node V was measured. Figure 2A shows the measured steady-state synaptic currents when V is clamped at $V = 5.0$ volts, and V_{pre} is swept from 0 to 5 volts. Figure 2B shows the measured steady-state synaptic currents when $V_{pre} = 5.0$ volts, and V is swept from 0 to 5 volts. The data shown in Figure 2A validate the sigmoid characteristic described in equation 2.13, and the data shown in Figure 2B correspond to the function describing the factor α_N (see equation 2.9).

It is interesting that when the system of two silicon neurons has had well-matched frequencies and the strength of coupling has been reduced to a value less than the smallest measurable I_{BSyn}, $I_{BSyn} < 3$ pA, the neurons have oscillated synchronously. This evidence supports the prediction derived from our mathematical model that this system demonstrates synchronous oscillations even if the strength of synaptic connection tends to zero. Nevertheless, it does not exclude the possibility that a parasitic electrotonic component of synaptic coupling might be responsible for this synchronizing effect.

To investigate whether a parasitic electrotonic component of synaptic coupling exists, the experiments described for Figures 2A and 2B were performed with all current sources (including I_{BSyn}) turned off; the results are shown in Figure 2C and Figure 2D, respectively. Figure 2D reveals leak currents that increase with an increase in the clamp voltage of the postsynaptic cell. These leak currents are due to a parasitic (reversed biased) diode present on the drain terminal of all MOS transistors. In an experiment corresponding to Figure 2A, we set the clamp voltage to $V = 0.3$ volts to minimize the effects of the leak currents described above. The result, shown

---

[1] The adjusted parameters used in the mathematical model are $I_{BL} = 48.0$ nA, $I_{BH} = 6.437$ nA, $I_\tau = 2.81$ nA, $I_{ext} = 15.0$ nA, $V_{High} = V_{dd} = 5.0$ volts, $V_{Low} = 0.0$ volts, $V_H = V_L = V_{thresh} = 2.0$ volts, and $C_1 = C_2 = 35$ pF.
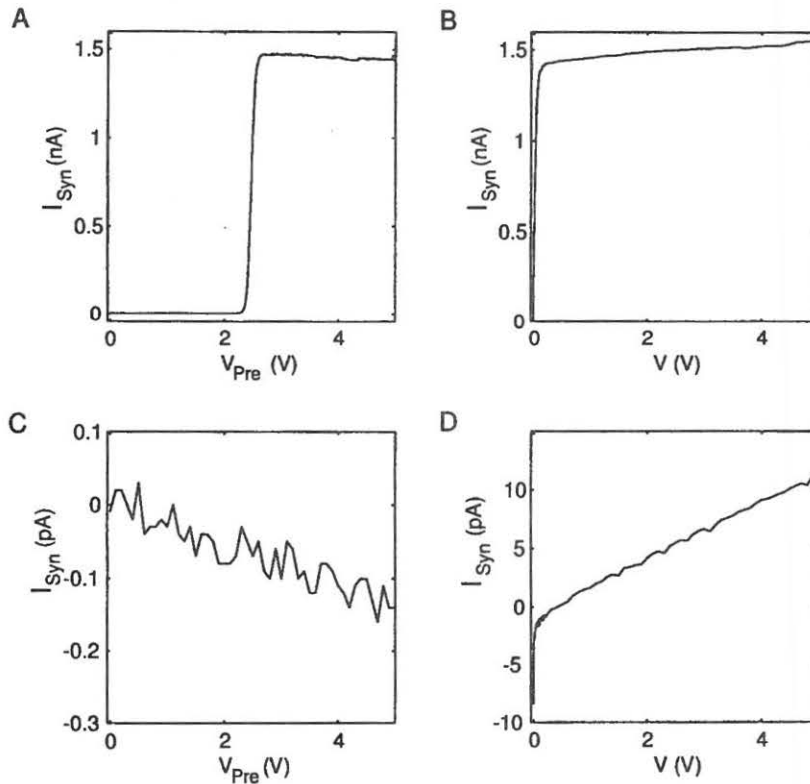
Figure 2: Experimental characterization of synaptic connection. (A) Synaptic current is presented with the membrane potential clamped at $V = 2.5$ volts, the presynaptic potential swept from 0.0 to 5.0 volts, and the synaptic weight set at $I_{BSyn} = 1.45$ nA. (B) The synaptic current is presented with the presynaptic potential clamped at $V_{pre} = 5.0$ volts, the membrane's clamp voltage swept from 0.0 to 5.0 volts, and the synaptic weight set at $I_{BSyn} = 1.45$ nA. In (C) and (D), the synaptic currents are presented under the same conditions as in (A) and (B), respectively; however, I_{BSyn} has been turned off.

in Figure 2C, demonstrates that very weak electrotonic coupling does exist (approximately 100 TΩ).

To investigate whether parasitic capacitive coupling exists, we measured the step response from V_{pre} to V, with all current sources turned off. Although small, there is a measurable amount of capacitive coupling between V and V_{pre}. For a 5-volt step in V_{pre}, the measured change in V is 26 mvolts, which corresponds to a coupling capacitance of approximately 50 fF.

4 Observed Behaviors as I_{BSyn} Is Varied

The mathematical model presented above and the silicon neurons show a number of similar stable oscillatory behaviors. In the mathematical model, we call a limit cycle stable if it is asymptotically stable. We evaluate the stability by calculating characteristic multipliers using the bifurcation analysis software LocBif (Khibnik, Kuznetsov, Levitin, & Nikolaev, 1993). In the silicon neuron experiments, our criterion for the stability of oscillations was that they persist in the presence of inherent noise and small voltage perturbations.

As we varied the strength of the inhibitory connections, I_{BSyn}, we observed the following corresponding stable oscillatory behaviors in both the silicon neuron experiments and the mathematical model (*experimental behavior–model behavior*):

synchronous oscillations (see Figure 3B)–synchronous limit cycle, *SC*

phase-shifted oscillations (see Figures 3A and 4A and 4B)–a pair of phase-shifted nonsymmetric limit cycles–NSC_1/NSC_2

alternating oscillations (see Figure 3C)–antiphase limit cycle, *AC*

drifting oscillations (see Figure 4C)–stable torus *T*

Here we do not present certain behaviors that are stable in the mathematical model but have not been observed experimentally. It is possible that these behaviors were not observed because the basin of attraction with the necessary initial conditions is so narrow. The model demonstrates different asymmetric limit cycles, where, for example, one model neuron oscillates with higher amplitude and half the frequency of the other (see Figures 5A and 5C). As another example, one model neuron may demonstrate small-amplitude spindle-like oscillations, and the other would oscillate with the waveform similar to that of an uncoupled oscillator (see Figures 5B and 5D). Due to the symmetry in the system, nonsymmetric oscillations always appear in pairs. For instance, in the case of Figures 5A and 5C, depending on initial conditions, one or the other neuron oscillates with the larger amplitude and the smaller frequency. It is interesting to note that Jung, Kiemel, and Cohen (1996) observed a similar pair of limit cycles in a model of lamprey segmental oscillator.

Comparison of Figures 6 and 8 to Figures 7 and 9 shows good qualitative correspondence between dynamic behaviors and transitions occurring in the systems when I_{BSyn} was varied. In the model, the synchronous limit cycle is stable for $I_{BSyn} \in [0, 0.140]$ nA. It loses stability at point a (see Figure 7), at the critical value $I_{BSyn} = 0.140$ nA, and undergoes a Neimark-Sacker torus bifurcation. In the mathematical model, a stable torus is observed at I_{BSyn} smaller than the critical value at point a. Therefore, we infer that this is a subcritical torus bifurcation, and a stable torus appears at a fold torus bifur-

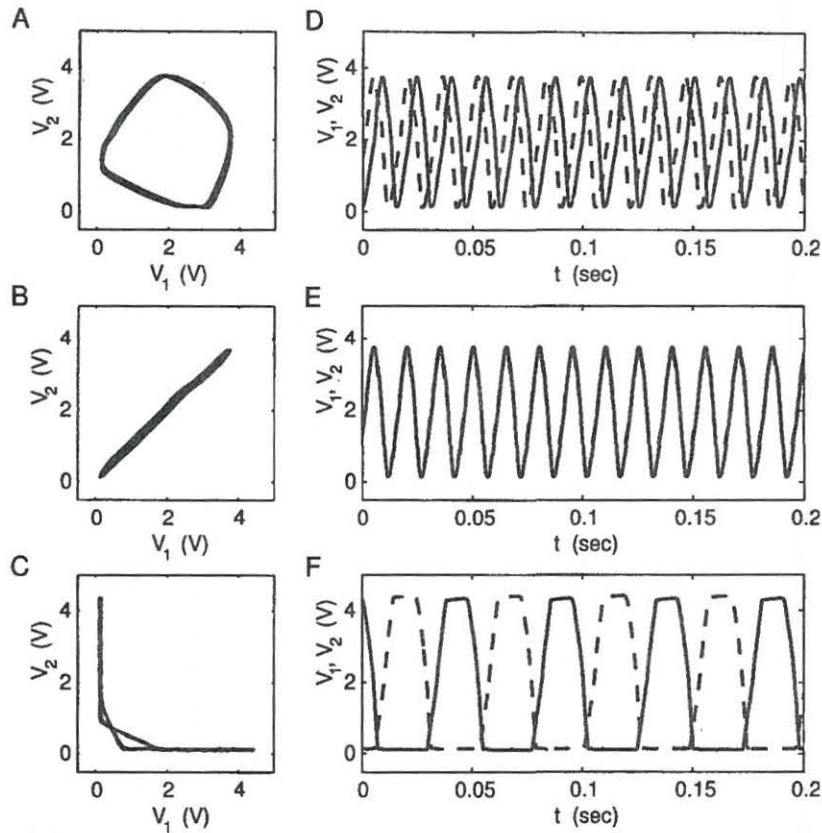Cymbalyuk, Patel, Calabrese, DeWeerth, & Cohen

Figure 3: Experimentally obtained oscillatory modes of the two silicon neurons connected by mutually inhibitory synapses. (A, D) Phase-shifted oscillations and (B, E) synchronous oscillations were both stable when the connections were of moderate value, ($I_{BSyn} = 1.4$ nA). By proper choice of initial conditions, one could choose the oscillatory mode observed. The alternating oscillations (C, F) were stable, if the connections were strong, ($I_{BSyn} = 1464.9$ nA). Here and in Figure 4, solid and dashed lines differentiate the membrane potentials of the two silicon neurons, V_1 and V_2. (A–C) Data collected during 3 seconds.

cation together with an unstable torus. Thus, for some values of I_{BSyn}, a stable torus coexists with the stable synchronous limit cycle and an unstable torus. At point a the unstable torus disappears, and synchronous oscillations lose stability. Similarly, in experiments with silicon neurons, synchronous oscillations were observed for the inhibitory connections ranging from zero up to moderate strengths of coupling, $I_{BSyn} = 2.70$ nA (see point a, Figure 6). Corresponding to the mathematical model, we observed drifting oscillations
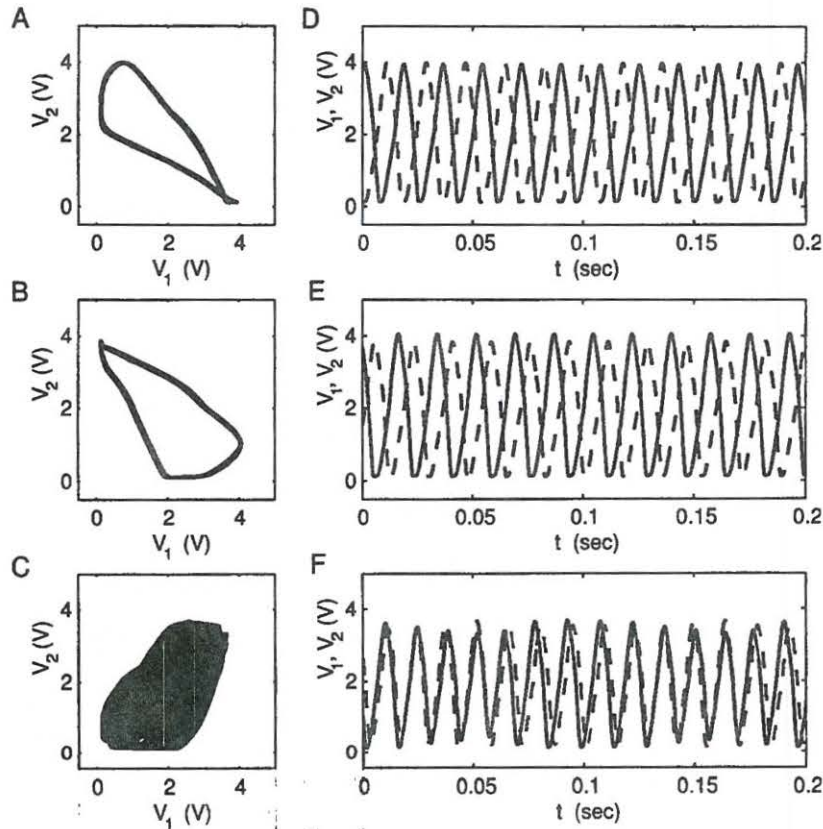
Figure 4: Experimentally obtained oscillatory modes of the two silicon neurons connected via inhibitory connections of moderate strength, $I_{BSyn} = 3.2$ nA. (A, B) Phase-shifted oscillations coexisted with (C) drifting oscillations.

coexisting with synchronous oscillations at I_{BSyn} close to the critical value. An example of the drifting oscillations for stronger coupling is presented at Figure 4C along with the pair of phase-shifted oscillations (see Figures 4A and 4B).

In the model for the moderate strength of synaptic coupling, the pair of stable phase-shifted limit cycles NSC_1/NSC_2 is observed, so that depending on the initial conditions, one or the other oscillator leads. For the parameters provided, we observed phase differences $\phi \in [0.33, 0.67]$. The NSC_1/NSC_2 appear at the fold bifurcation for limit cycles together with a pair of unstable phase-shifted limit cycles, $I_{BSyn} = 0.0564$ nA (see point b, Figure 7) and disappear at the pitchfork limit cycle bifurcation, $I_{BSyn} = 6.511$ nA (see point c, Figure 7), where NSC_1 and NSC_2 merge and AC becomes stable. Similar
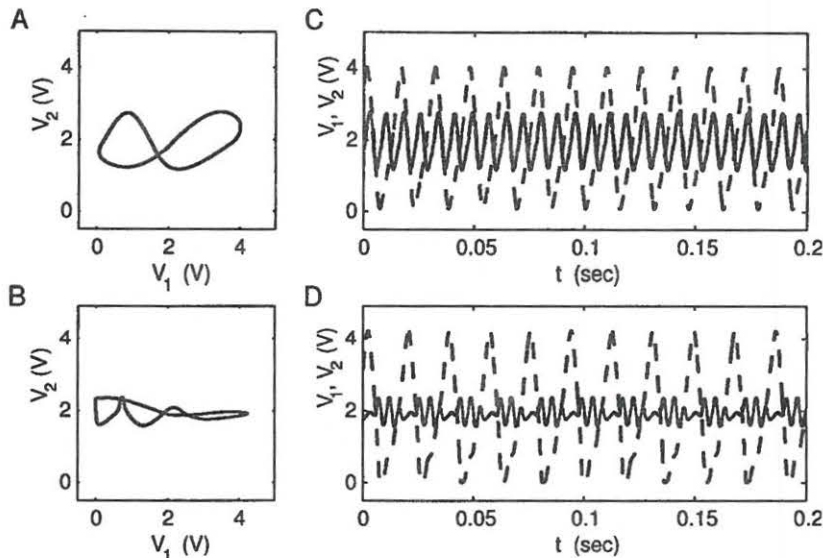
Figure 5: Examples of stable, nonsymmetric limit cycles obtained from the mathematical model of the two symmetrically inhibitory coupled identical silicon neurons. These limit cycles were not observed in experiments. (A, C) One of the two oscillators demonstrates 2.5 times larger amplitude and twice as large period, representing 1:2 synchronization mode: $V_1 = 3.52888$ volts, $W_1 = 1.87397$ volts, $V_2 = 1.72983$ volts, $W_2 = 1.79920$ volts, $I_{BSyn} = 1.9947$ nA. (B, D) One of the two oscillators shows high-amplitude oscillations, and the other shows small-amplitude "spindle" oscillations: $V_1 = 3.15062$ volts, $W_1 = 1.79645$ volts, $V_2 = 1.75655$ volts, $W_2 = 1.89334$ volts, $I_{BSyn} = 11.9122$ nA.

behaviors were observed experimentally. For sufficiently strong synaptic connections, we observed only alternating oscillations. As we made the strength of the connections weaker, at $I_{BSyn} \approx 6.34$ nA (see point c in Figure 6), two phase-shifted oscillations branched from the alternating oscillations, which became unstable for the weaker coupling. As I_{BSyn} decreased to $I_{BSyn} \approx 1.51$ nA, the phase difference between oscillations went from $\phi = 0.50$ (for alternating oscillation) to $\phi \approx 0.22$ ($\phi \approx 0.76$ for the other branch).

The model and experimental data have qualitatively similar dependencies of the amplitude (compare Figure 8A and Figure 9A) and the period (compare Figure 8B and Figure 9B) on the strength of coupling. Synchronous oscillations in both cases have amplitude and period close to the corresponding values in the uncoupled system. Phase-shifted oscillations lay on the transition from synchronous oscillations to alternating oscillations. Our silicon neurons also demonstrated that stronger inhibitory synaptic con-
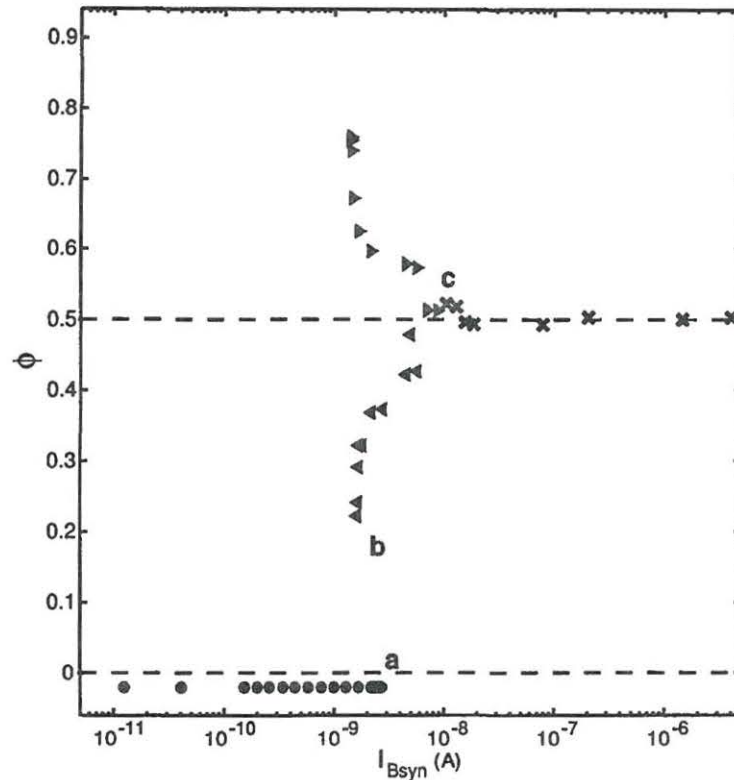
Figure 6: Experimentally obtained bifurcation diagram for the two mutually inhibitory silicon neurons. The phase difference, ϕ, of different phase-locked oscillations is plotted against strength of the synaptic connections, I_{BSyn}. Synchronous oscillations are stable for weak coupling and give rise to stable drifting oscillations at the moderate strength of coupling a ($I_{BSyn} = 2.70$ nA). A pair of phase-shifted oscillations appeas at point b ($I_{BSyn} \approx 1.40 \div 1.62$ nA), is stable for moderate strengths of coupling, and gives stability to alternating oscillations, merging at point c ($I_{BSyn} \approx 5.62 \div 7.06$ nA). Alternating oscillations remain stable for the strong inhibitory connections. Here and in Figure 7, circles, triangles, and X's represent synchronous oscillations, phase-shifted oscillations, and alternating oscillations, respectively.

nections produced slower oscillations (see Figures 8B and 9B), reproducing qualitatively the frequency dependence observed in strychnine experiments in the lamprey (Cohen & Harris-Warrick, 1984; Grillner & Wallen, 1980).

Under the condition of identical intrinsic periods of our silicon neurons, we observed synchronous oscillations experimentally in the absence
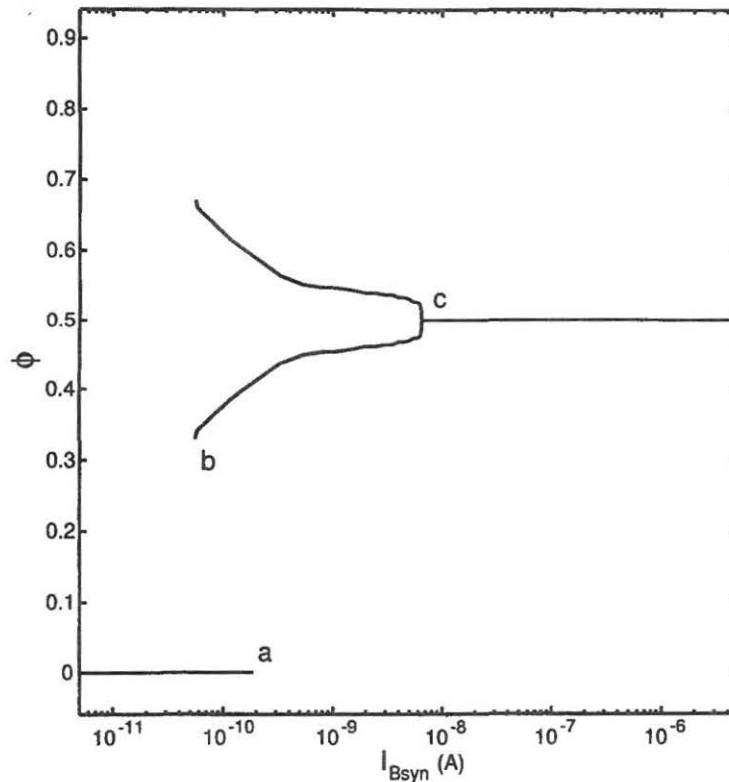
Figure 7: The bifurcation diagram of phase-locked oscillations obtained for the mathematical model of the two symmetrically inhibitory coupled identical oscillators as strength of connection, I_{BSyn}, is varied. The synchronous limit cycle, stable with weak coupling, became unstable at a subcritical Neimark-Sacker torus bifurcation at moderate coupling strength at point a ($I_{BSyn} = 0.140$ nA). The pair of stable nonsymmetrical phase-shifted limit cycles NSC_1/NSC_2 appears along with the pair of unstable nonsymmetrical phase-shifted limit cycles $UNSC_1/UNSC_2$ at fold bifurcation for limit cycles at point b, $I_{BSyn} = 0.0564$ nA. Antiphase limit cycle is stable for the strong inhibitory connection and loses stability on the pitchfork limit cycle bifurcation, giving stability to the pair of phase-shifted limit cycles NSC_1/NSC_2 at point c ($I_{BSyn} = 6.511$ nA).

of synaptic coupling. To eliminate the possibility that synchronization appears primarily due to parasitic electrotonic coupling, we investigated the system with approximately 2% disparity in the intrinsic oscillation periods such that phase locking was disrupted and drifting oscillations ensued. By adding weak inhibitory coupling, we were then able to return the circuit to
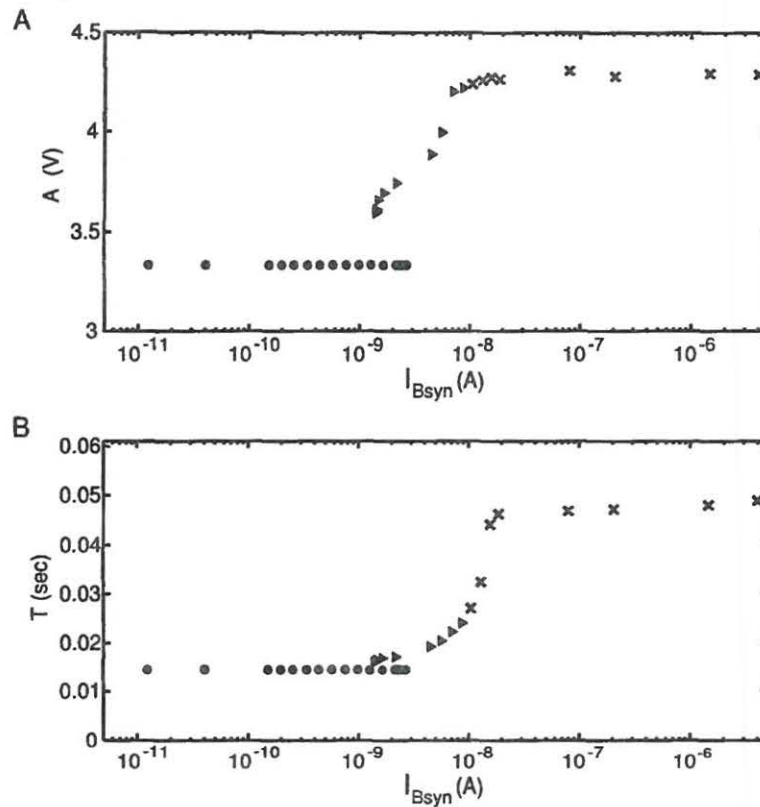
Figure 8: Experimentally observed amplitude and period of phase-locked oscillations of the two mutually inhibitory silicon neurons. The (A) amplitude, A, and the (B) period, T, of the oscillations are shown against strength of synaptic connection, I_{BSyn}.

stable synchronous oscillations. Thus, inhibitory coupling can synchronize mismatched oscillators that parasitic coupling, even if it exists, is too weak to synchronize. Note that our conclusion—synchronous oscillations are maintained by weak inhibitory coupling—is also supported by the mathematical model, which exhibited synchronous oscillations even for negligibly small coupling.

5 Discussion

We have described a pair of coupled silicon neurons implemented using VLSI technology and compared experimental results from these neurons to
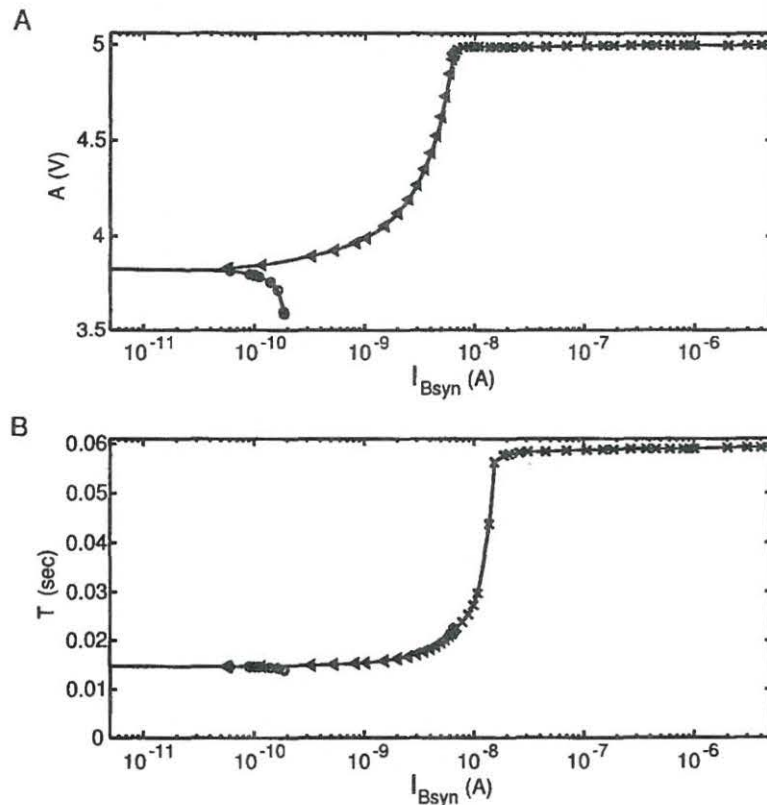
Cymbalyuk, Patel, Calabrese, DeWeerth, & Cohen

Figure 9: Amplitude and period of phase-locked oscillations obtained for the mathematical model of the two symmetrically inhibitory coupled identical oscillators as strength of connection, I_{BSyn}, is varied. Circles, triangles, and X's represent the synchronous limit cycle, phase-shifted limit cycle, and antiphase limit cycle, respectively.

simulation data from a corresponding mathematical model. In particular, we have shown that the silicon circuits can replicate many of the dynamical regimes seen in a mathematical model. Thus, silicon neurons can be used to demonstrate that these mathematically predicted behaviors can exist stably in real-world systems.

The described results point to a role for inhibitory connections in the generation of rhythmic behavior in biological CPGs. In the spinal CPG network of the lamprey, for example, segmental oscillators normally produce alternating oscillations. However, when bathed in strychnine, synchronous oscillations replace the alternating oscillations. It is known that

strong contralateral inhibitory (glycinergic) connections, which can be blocked by strychnine, exist in the CPG network. It has been proposed that the transition from alternating to synchronous oscillations can be accounted for by weak contralateral excitatory connections (Cohen & Harris-Warrick, 1984; Alford et al., 1989). The strychnine-dependent transition may be due to changes in the relative strength of excitatory and inhibitory connections, that is, the left and right oscillators are connected by relatively strong reciprocal inhibitory connections parallel to comparatively weaker reciprocal excitatory coupling (Cohen & Harris-Warrick, 1984; Alford et al., 1989).

While it is known that a few neurons with crossed excitatory connections do exist, the results shown here demonstrate that there is an alternative explanation for the phase transition. We suggest that the simplest explanation is that inhibitory connections alone can produce the observed transition. In addition, electrotonic coupling between the left and right oscillatory neurons may exist and produce synchronous oscillations when inhibitory connections are weak or disrupted by strychnine. Moreover, it has been shown in a mathematical model that electrotonic coupling alone can, under some conditions, reproduce the transition from synchronous to alternating oscillations in a circuit of two coupled Hindmarsh-Rose neurons (Cymbalyuk et al., 1994). There are three basic hypotheses that can account for the influence of strychnine on the dynamical behavior of the spinal CPG:

1. The inhibitory connections produce stable alternating oscillations when they are strong and synchronous oscillations when they are sufficiently weak (in particular, when they are under the influence of strychnine).

2. The inhibitory connections are accompanied by the electrical connections, which can produce synchronous oscillations when inhibitory connections are weak or blocked.

3. If inhibitory connections are strong and excitatory connections are weak, then as inhibitory connections are blocked, excitatory connections become relatively stronger, facilitating stable synchronous oscillations.

These hypotheses are complementary in the sense that all may be valid simultaneously. The first two hypotheses have not been proposed previously. They appear, however, to be the most biologically plausible.

It is also interesting to note that the quasi-periodic behavior observed in our silicon model experiments and mathematical model might conform to experiments with the lamprey. Lesher et al. (1998) have shown that lamprey spinal central pattern generators might employ a chaos control mechanism based on a skeleton of unstable oscillations. According to this mechanism, the CPGs exhibit unstable oscillations rather than stable oscillations. It is synaptic connectivity or control signals that appear to provide stability to

the desired regime. In future work, the systems of silicon neurons could give some insight to the potential for this control mechanism.

We are developing a variety of silicon neurons and associated systems of neurons that implement biologically inspired motor behaviors such as axial locomotion (DeWeerth, Patel, Simoni, Schimmel, & Calabrese, 1997; Patel, Holleman, & DeWeerth, 1998). These efforts are directed at the creation of dynamical sensorimotor systems that exhibit tightly coupled sensory feedback and motor learning, providing platforms for both testing biological hypotheses and addressing engineering applications. A major challenge in this development lies in the derivation of mathematical models that facilitate qualitative and quantitative understanding of the complex behaviors of these systems. The modeling of individual silicon neurons and circuits, as exemplified by this article, provides the foundation for this effort.

Acknowledgments

References

Alford, S., Sigvardt, K. A., & Williams, T. L. (1990). GABAergic control of rhythmic activity in the presence of strychnine in the lamprey spinal cord. *Brain Research, 506*, 303–306.

Blechman, I. I. (1981). *Synchronization in nature and engineering*. Moscow: Nauka. (In Russian).

Borisyuk, G. N., Borisyuk, R. M., Khibnik, A. I., & Roose, D. (1995). Dynamics and bifurcations of two coupled neural oscillators with different connection types. *Bulletin of Mathematical Biology, 57*, 809–840.

Bush, P., & Sejnowski, T. (1996). Inhibition synchronizes sparsely connected cortical neurons within and between columns in realistic network models. *J. Computational Neuroscience, 3*, 91–110.

Chow, C. C., White, J. A., Ritt, J., & Kopell, N. (1998). Frequency control in synchronized networks of inhibitory neurons. *J. Computational Neuroscience, 5*, 407–420.

Cohen, A., & Harris-Warrick, R. M. (1984). Strychnine eliminates alternating motor output during fictive locomotion in the lamprey. *Brain Research, 293*,

164–167.

Cymbalyuk, G. S., Nikolaev, E. V., & Borisyuk, R. M. (1994). In-phase and anti-phase self-oscillations in a model of two electrically coupled pacemakers. *Biological Cybernetics, 71*, 153–160.

Destexhe, A., Contreras, D., Sejnowski, T. J., & Stereade M. (1994). A model of spindle rhythmicity in the isolated thalamic reticular nucleus. *J. Neurophysiology, 72*, 803–818.

DeWeerth, S. P., Patel, G. N., Simoni, M. F., Schimmel, D. E., & Calabrese, R. L. (1997). A VLSI architecture for modeling intersegmental coordination. In R. Brown & A. Ishii (Eds.), *Proceedings of the 17th Conference on Advanced Research in VLSI* (pp. 182–200). New York: IEEE Computer Society.

Ermentrout, G. B. (1996). Type I membranes, phase resetting curves, and synchrony. *Neural Computation, 8*, 979–1001.

Ermentrout, G. B., & Kopell, N. (1991). Multiple pulse interactions and averaging in systems of coupled neural oscillators. *J. Mathematical Biology, 29*, 195–217.

Gerstner, W., van Hemmen, J. L., & Cowan, J. D. (1996). What matters in neuronal locking? *Neural Computation, 8*, 1653–1676.

Golomb, D., Wang, X.-J., & Rinzel, J. (1994). Synchronization properties of spindle oscillations in a thalamic reticular nucleus model. *J. Neurophysiology, 72*, 1109–1126.

Grillner, S., & Wallen, P. (1980). Does the central pattern generation for locomotion in lamprey depend on glycine inhibition? *Acta Physiol Scand, 110*, 103–105.

Hansel, D., Mato, G., & Meunier, C. (1995). Synchrony in excitatory neural networks. *Neural Computation, 7*, 307–337.

Hoppensteadt, F. C., & Izhikevich, E. M. (1997). *Weakly connected neural networks.* New York: Springer-Verlag.

Izhikevich, E. M. (1999). Weakly pulse-coupled oscillators, FM interactions, synchronization, and oscillatory associative memory. *IEEE Transactions on Neural Networks, 10*, 508–526.

Jung, R., Kiemel, T., & Cohen A. H. (1996). Dynamic behavior of a neural network model of locomotor control in the lamprey. *J. Neurophysiology, 75*, 1074–1086.

Khibnik, A. I., Kuznetsov, Yu. A., Levitin, V. V., & Nikolaev E. V. (1993). Continuation techniques and interactive software for bifurcation analysis of ODEs and iterated maps. *Physica D, 62*, 360–367.

Kuramoto, Y. (1984). *Chemical oscillations, waves and turbulence.* New York: Springer-Verlag.

Lesher, S., Spano, M. L., Mellen, N. M., Guan, L., Dykstra, S., & Cohen, A. H. (1998). Evidence for unstable periodic orbits in intact swimming lampreys, isolated spinal cords, and intermediate preparations. *Ann NY Acad Sci., 16*, 486–491.

Lytton, W., & Sejnowski, T. (1991). Simulations of cortical pyramidal neurons synchronized by inhibitory neurons. *J. Neurophysiology, 66*, 1059–1097.

Mahowald, M. A., & Douglas, R. (1991). A silicon neuron. *Nature, 354*, 515–518.

Malkin, I. G. (1956). *Some problems of the theory of nonlinear oscillations.* Moscow: Gostehizdat.

Mead, C. A. (1989). *Analog VLSI and neural systems*. Reading, MA: Addison-Wesley.

Morris, C., & Lecar, H. (1981). Voltage oscillations in the barnacle giant muscle fiber. *Biophysical Journal, 35,* 193–213.

Patel, G. N., Cymbalyuk, G. S., Calabrese, R. L., & DeWeerth, S. P. (1999). Bifurcation analysis of a silicon neuron. In *Proceedings of the NIPS '99.*

Patel, G. N., & DeWeerth, S. P. (1997). An analogue VLSI Morris-Lecar neuron. *Electronics Letters, IEE, 33,* 997–998.

Patel, G. N., Holleman, J. H., & DeWeerth, S. P. (1998). Analog VLSI model of intersegmental coordination with nearest-neighbor coupling. In M. Jordan, M. Kearns, & S. Solla (Eds.), *Advances in neural information processing, 10* (pp. 719–725). Cambridge, MA: MIT Press.

Rinzel, J., & Ermentrout, B. (1998). Analysis of neural excitability and oscillations. In C. Koch & I. Segev (Eds.), *Methods in neuronal modeling: From ions to networks* (2nd ed.) (pp. 251–191). Cambridge, MA: MIT Press.

Rubin, J. E., & Terman, D. (2000). Geometric analysis of population rhythms in synaptically coupled neuronal networks. *Neural Computation, 12,* 597–645.

Skinner, F. K., Turrigiano, G. G., & Marder, E. (1993). Frequency and burst duration in oscillating neurons and two-cell networks. *Biological Cybernetics, 69,* 375–383.

Terman, D., Kopell, N., & Bose, A. (1998). Dynamics of two mutually coupled slow inhibitory neurons. *Physica D, 117,* 241–275.

Van Vreeswijk, C., Abbot, L. F., & Ermentrout, G. B. (1994). When inhibition not excitation synchronizes neural firing. *J. Computational Neuroscience, 1,* 313–321.

Wang, X. J., & Rinzel, J. (1992). Alternating and synchronous rhythms in reciprocally inhibitory model neurons. *Neural Computation, 4,* 84–97.

Wang, X. J., & Rinzel, J. (1993). Spindle rhythmicity in the reticularis thalami nucleus: Synchronization among mutually inhibitory neurons. *Neuroscience, 53,* 899–904.

White, J., Chow, C. C., Ritt, J., Soto-Treviño, C., & Kopell, N. (1998). Synchronization and oscillatory dynamics in heterogeneous, mutually inhibited neurons. *J. Computational Neuroscience, 5,* 5–16.